Mechanical Characterisation of Interpenetrating Network Metal Ceramic Composites

F. Scherm[1], R. Völkl[1], A. Neubrand[2], F. Bosbach[3], U. Glatzel[1]

[1] Metals and Alloys, University Bayreuth, D-95440 Bayreuth, Germany

[2] Fraunhofer Institut für Werkstoffmechanik, D-79108 Freiburg, Germany

[3] Department of Engineering Design and CAD, University Bayreuth, D-95440 Bayreuth, Germany

Abstract

A variety of interpenetrating light weight metal matrix composites (porous Al_2O_3 preforms infiltrated with the aluminium alloy AlSi9Cu3) have been characterised under tensile und compressive loads and fractographically examined by scanning electron microscopy. Fatigue and thermophysical properties were determined. Compared to die-cast AlSi9Cu3, the mechanical properties of the interpenetrating composites were significantly improved:

- the elastic modulus increased more than twofold
- the tensile strength increases by a factor of 2
- fatigue limits increased by a factor of 2.3-2.6
- density increased slightly by a factor of 1.2
- thermal conductivity is reduced by a factor of 0.5

Keywords

Metal matrix composites, stiffness, strength, fatigue, thermophysical properties

Introduction

Metal matrix composites (MMCs) have gained interest in recent years because of their outstanding properties. Demanding specifications from automotive and aerospace industry concerning fuel efficiency and emission standards on the one hand, and high standards concerning comfort and safety on the other hand are the motivation for decreasing vehicle weight by using MMCs. The main development objectives for MMCs are an increase in stiffness, yield strength, tribological and elevated temperature properties of light metals. The classification of MMCs occurs by the type of the ceramic components used for reinforcement such as particle, whisker and fibre, and multidirectional network structures, showing an interpenetrating structure [1-4].

Most work on MMCs has concentrated on particle or fibre reinforced composites in which the ceramic phase is not continuous [5]. While long fibre reinforced MMCs can have excellent mechanical properties, they are very expensive so far due to the high cost of ceramic fibres. Much lower production costs can be achieved by dispersing SiC particles in aluminium [6] or magnesium [7] melts followed by a casting, extrusion or forging process – see Ref. [8] for a review. However, the ceramic content of cast particle composites is limited, their microstructure can be difficult to control and they inherently provide only a moderate stiffness increase [9]. In cases where ductility is not of concern, metal matrix composites with interpenetrating network microstructures offer a better control of the distribution of the ceramic phase and more ceramic-like properties (i.e. higher stiffness, lower thermal expansion). Interpenetrating network metal MMC are usually fabricated by pressure assisted [5] or spontaneous infiltration [10] of open porous ceramic preforms [11]. In this paper, it will be demonstrated that Al_2O_3 based interpenetrating composites with 40-50 vol.% metal content not only offer unusually high stiffness, but also favourable fatigue properties .

Experimental

Materials

All investigated MMCs were prepared by die casting of different ceramic preforms of 200 × 90 × 30 mm^3 size with the Al alloy AlSi9Cu3 (max. 1.3 wt.% Fe, max. 0.55 wt.% Mn). The density of 2.75 g/cm^3 and E-modulus of 75 GPa of the alloy are taken from [12]. The preforms A and B were chosen out of 17 different preforms and were produced by cold pressing fine grained ceramic alumina powders containing pyrolysable pore formers followed by burnout and partial sintering. The processing parameters were chosen in such a way that preforms with similar porosities between 52 and 55% were produced. The Al_2O_3-preforms A and B had different pore diameters (0.5 µm for A and 2.0 µm for B), porosities which were measured by mercury porosimetry, were 55% for preform A and 52% for preform B.

Metal matrix and ceramic reinforcement were both isotropic distributed in all samples of this study. Under special circumstances the ceramic preform was compressed on one side but these samples were not investigated further. More information on the processing principle of the preforms can be found in [9], the microstructure of these MMCs is described in detail in [13].

Mechanical Characterization

Specimens for tensile testing were fabricated by water-jet cutting, cylindrical grinding and precision turning using polycrystalline diamond tools. The specimens for fatigue testing were additionally ground and polished. The average surface roughness R_a of all tensile specimens was determined by profilometric measurements and was better than 2 µm. The geometry of the specimens for tensile tests was cylindrical with 5 mm gauge diameter and 12 mm grip

diameter with 39 mm transition radii to ensure that all tensile failures occur within the gauge length of 20 mm. The overall length of the specimens was 140 mm. The fatigue specimens were smaller with 9 mm grip diameter, 4 mm gauge diameter, 21 mm transition radii, 10 mm gauge length with and an overall length of 68 mm. The specimens used for compressive tests were of cylindrical shape, with 24 mm length and 12 mm diameter.

Tensile and compression tests were performed using a Zwick Z100/TL3S tensile testing machine, with hydraulic specimen grips, in case of tension and with polished and lubricated plates in case of compression tests. The fatigue tests were carried out on a MTS 851 servohydraulic testing machine. The strain was measured by clip-on extensometers attached directly to the gauge length, with a resolution of 0.6 μm, for tension and compression tests. Young`s moduli were determined by acoustic resonance method and from stress strain curves (which is indicated within the Figures or Tables).

Fractographic examinations of crack surfaces of tested tensile and compression specimens were conducted, using scanning electron microscopy (SEM, Zeiss 1540 XB). The SEM was equipped with an Noran System Six EDX analyser.

The thermophysical properties thermal diffusitivity, coefficient of thermal expansion and specific heat capacity were measured by laser flash method (Netzsch LFA 427), dilatometry (Netzsch DIL 402C) and differential scanning calorimetry (Netzsch DSC 204) in temperature range from room temperature up to 450 °C. For thermal diffusivity measurements the sample surface was coated with a thin carbon layer to improve absorption of the laser radiation. The thermal diffusivity measurements were carried out under isothermal conditions: the temperature was increased from room temperature to test temperature and then kept constant for at least 15 min. Evaluation of the acquired data was performed using the half-time method described in [14].

Results and Discussion

Tensile Behaviour

Static tensile tests were performed on at least five specimens manufactured from the composites A and B. Figure 1 shows representative stress-strain curves for composites A and B. Linear elastic regions have been approximated at stresses below 50 MPa. At higher stresses the stress-strain behavior is even more non-linear for all tested composites under static load.

The non-linear behaviour of the composites is agreement with observations of Daehn et al. on interpenetrating MMCs [15]. They found that for small strains the cyclic stress-strain curves exhibit a linear behaviour, whereas for higher loads the behaviour changed to non-linear. This behaviour can be explained by the combination of an elastic deformation of the ceramic preform accompanied by a plastic deformation of the metal at higher stresses. It is difficult to determine a yield stress for these materials with good enough reproducibility. The 0.02% yield stress was determined using the Young`s modulus measured with acoustic resonance technique.

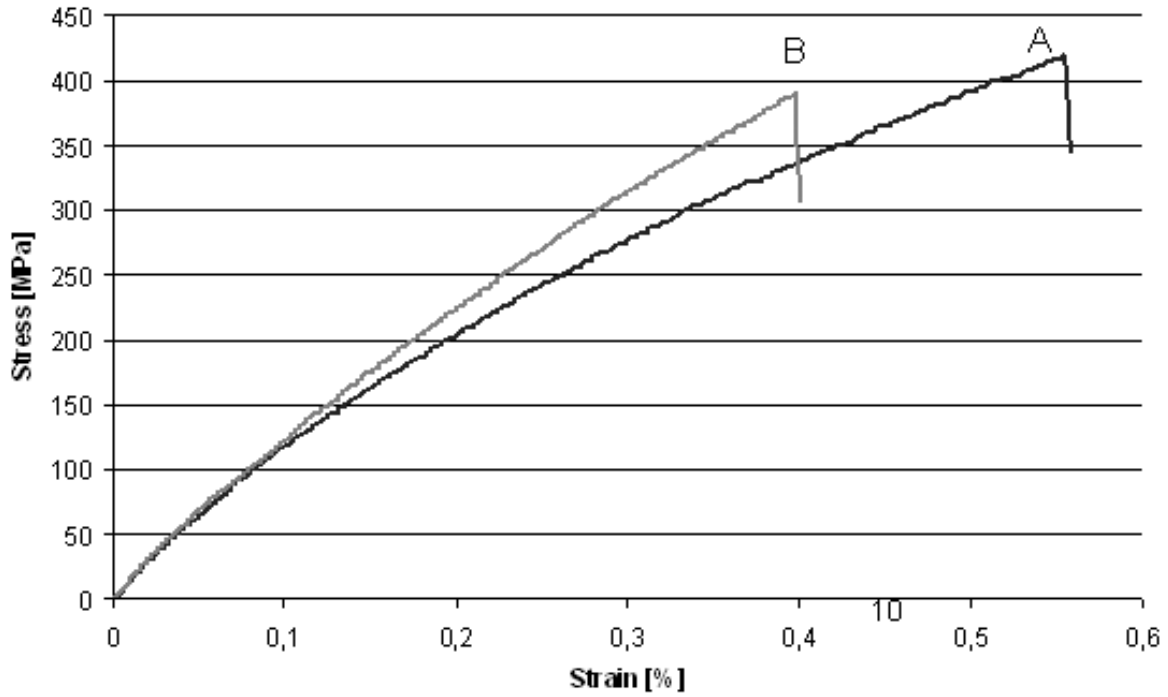

Figure 1: Stress-strain curves for composites A and B

The ultimate tensile strength (UTS) of these composites reached values beyond 400 MPa with a fracture strain around 0.5%. Depending on casting conditions, unreinforced AlSi9Cu3 [16-12] has an UTS from 200-310 MPa and a fracture strain from 0.5 to 3%. Hence, all composites, are considerably stronger and slightly less ductile than the unreinforced alloy. The basic mechanical properties of composites A and B are summarized in Table 1.

A large number of strengthening mechanisms has been identified in MMCs. They include stress transfer from the less stiff metal matrix to the stiff ceramic phase, dislocation strengthening, strengthening by refinement of the metal grain size amongst others [17]. Usually, these mechanisms act simultaneously, where the amount of strengthening of each mechanism differs from composite to composite. While no systematic study will be undertaken here to elucidate the exact contributions of different strengthening mechanisms, the experimental data provide already some insight. Composite B has a coarser microstructure and slightly higher ceramic content compared to composite A. The coarser microstructure

should lead to less dislocation strengthening [17] and thus a lower yield strength. This effect seems to be counterbalanced by a slightly higher ceramic content, so that the yield strength is similar to composite A. The ultimate strength of composite B is slightly lower as it behaves more brittle and has a lower fracture strain.

The interpenetrating network composites have in general a significantly higher elastic modulus when compared to Duralcan F3D.20S, and more than twice the modulus of AlSi9Cu3. The SiC reinforcements Duralcan and the alumina reinforcements in composite A und B have almost the same Young's modulus of about 415 GPa [18, 19], hence the different moduli must be due to microstructural differences. Indeed, it has been demonstrated earlier that interpenetrating metal-ceramic microstructures are considerably stiffer than ceramic particle reinforced metals at a given ceramic content [9]. Composite A has a substantially higher specific stiffness than the matrix alloy, i.e. $(E/\rho)_{composite} / (E/\rho)_{Al\ alloy} \approx 1.8$. The module to density ratio determines the velocity of sound and thereby the acoustic resonances of components. This high stiffness to density ratio is therefore not only advantageous for light weight structures, but can also be helpful for the acoustic design of components.

Table 1: Tensile properties, density and dynamic Young's modulus determined for the composites A and B, together with literature data for Duralcan F3D.20S and the matrix alloyAlSi9Cu3 [12-16, 20].

Preform type	Ultimate tensile strength [MPa]	0.02% yield strength [MPa]	Strain to failure [%]	Young's Modulus [GPa]	Density [g/cm³]
A	407 ± 42	95	0.53 ± 0.09	155	3.24
B	380 ± 16	97	0.39 ± 0.02	167	3.27
Duralcan F3D.20S	352 ± 56		0.4	94	2.82
AlSi9Cu3	200 – 310		0.5 – 3.0	75	2.75

Cyclic tension tests ware conducted for further characterisation of composite A. The samples were loaded in the first cycle until a stress of 75 MPa, then unloaded to a stress of 10 MPa. In the following cycles the maximum applied stress was increased in 25 MPa steps. The measurements were conducted in a single experiment; therefore the strain of the previous cycle was added to the actual cycle. An example for the stress-strain curves of these cyclic experiments is given in Figure 2.

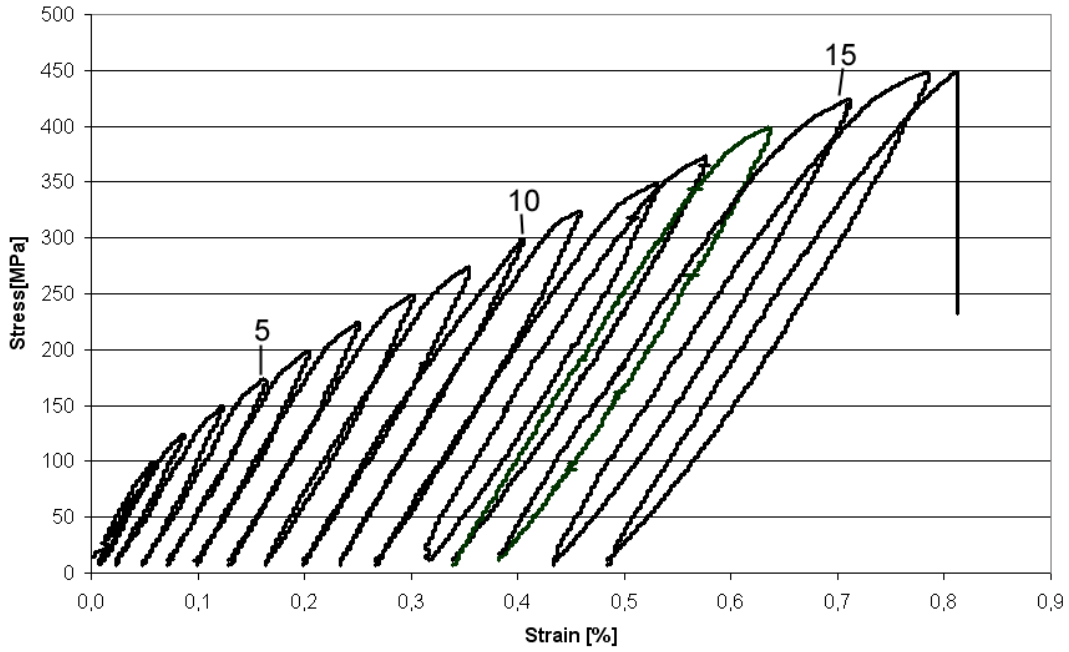

Figure 2: Stress-strain curves for cyclic load/unload experiments, specimen of type A

The failure of the sample occurred in cycle number 17 at 448 MPa stress and 0.5% strain. Hysteresis loops for cycle number 5, 10 and 15 are marked. They broaden with increasing cycle numbers and stresses.

Pseudo elastic modulus, was determined from the stress-strain curves by fitting secants in the hysteresis loops, decreases from a value of 152 GPa, for the first cycles to 140 GPa, for the last cycle. This tendency gives hints for an increasing an-elastic effect of the material at higher loads. A possible explanation can be seen in the growth of microcracks with increasing cycle number. The dynamic elastic modulus of composite A determined by acoustic resonance measurements was 155 GPa which is in good agreement with the modulus determined for low quasistatic deformations.

Compression Behaviour

Figure 3 shows tension behaviour of composite A in comparison to its compression behaviour. Measured values for compressive strength were approximately 850 MPa with 2% compressive strain. The ultimate compressive strength is thus about 2 times higher than the UTS, the strain to failure for compression is about 4 times higher than for tension. The non-linear stress strain behaviour, which was observed in tensile tests was also found in the compression tests. At moderate-high stresses strains the interpenetrating composites show less strain in compression than in tension. This tensile-compressive yielding anomaly has also been observed in whisker and long fibre reinforced composites and is generally attributed to residual stresses (i.e. the matrix is pre-strained in tension after cooling from the manufacturing temperature).

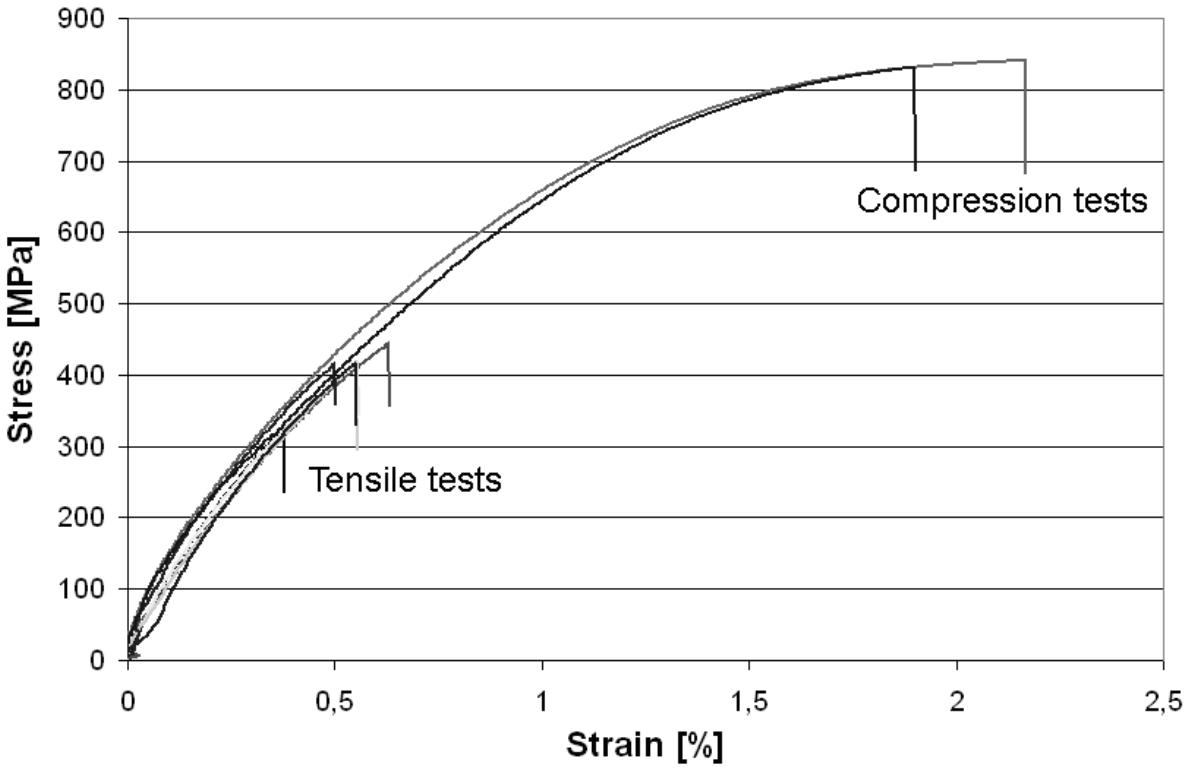

Figure 3: Stress-strain curves under tensile and compressive load, composite A sample

Fractographic Examinations

Characteristic for the observed fracture surfaces at a macroscopic scale is the absence of significant plastic deformation (Figure 4). The fracture plane was perpendicular to the applied load, in case of tensile experiments, therefore normal stress lead to materials failure. In case of compressive tests, the samples show a brittle fracture as a result of maximum shear stresses, leading to a fracture angle of 45°.

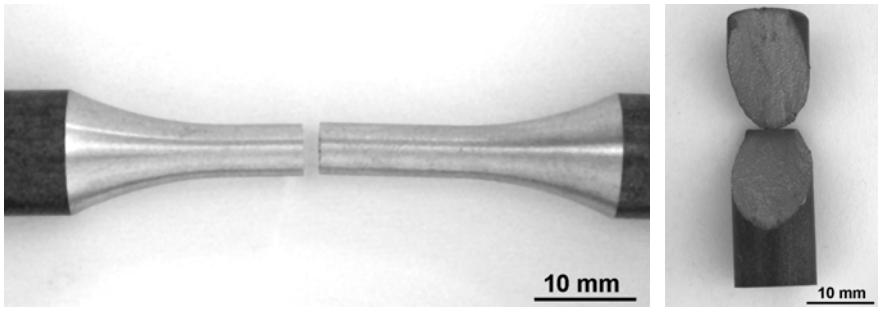

a) b)

Figure 4: Macroscopical images of tested specimens under a) tensile and b) compressive load (upper fractured part rotated by 180°) showing no plastic deformation

At a microscopic scale, the fracture surfaces of specimens from tensile tests, shown in Figure 5a) were dominated by dimples caused by ductile deformation of the metallic phase. The diameter of the dimples varied from 1 to 4 µm. Ceramic preforms failure was observed by cracking of the reinforcement in a brittle manner (indicated by an arrow in Figure 5a). The reinforcements cracked mainly parallel to the fracture plane.

The fracture surfaces of specimens tested under compressive loads, shown in Figure 5b) show a flaked structure, cracks and furrows caused by exposed ceramic particles which were pulled out of the composites and slid over the fracture surfaces after failure has occurred.

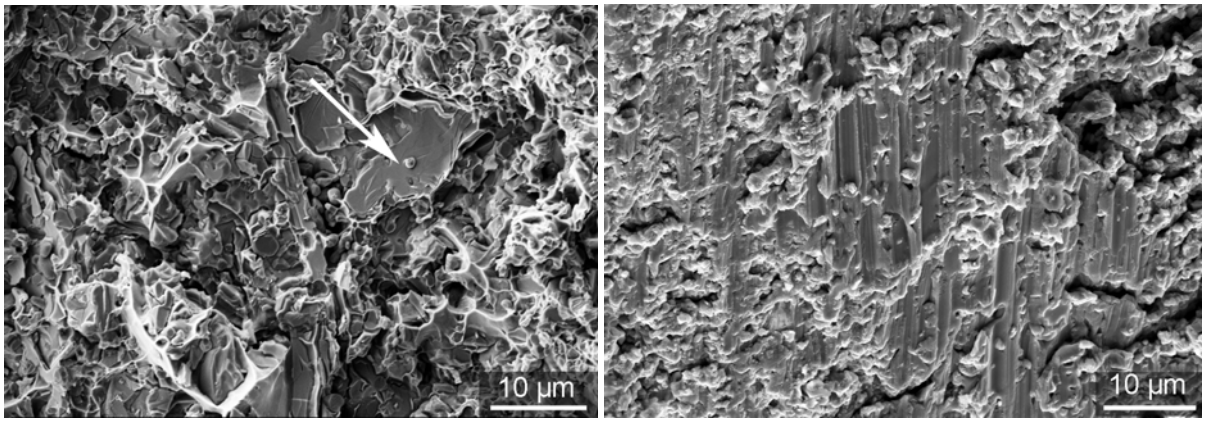

a) b)

Figure 5: SEM images, materials failure under tensile a), and compressive load, b)

Figure 6 shows a SEM image of a longitudinal section of a tested specimen under tensile load. The damage is confined to a very narrow band near the fracture plane. Even after severe plastic deformation the matrix is not debonded from the preform, matrix remnants attached to the preform are visible. Figure 6 also reveals cracking of the reinforcement, indicating that the interfacial bond strength between Al-matrix and Al_2O_3 preform is strong enough to withstand a high stress concentration at the interface, which is in good agreement with earlier microstructural observations by Zhou et al. [21].

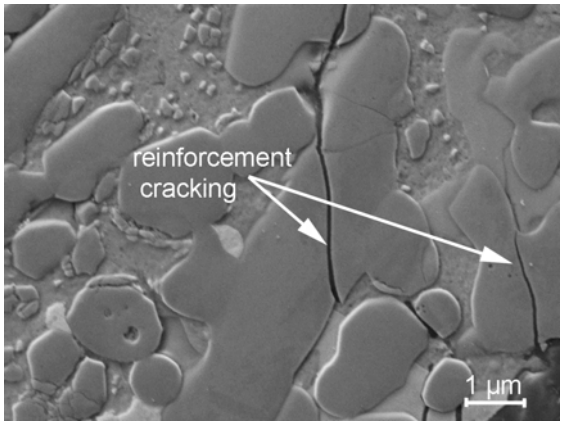

Figure 6: SEM image of longitudinal section: materials failure under tensile load, damage confined to a narrow band, reinforcement cracking is visible.

Fatigue Tests

Cyclic fatigue tests were carried out at room temperature and at 150°C. The ratio of applied maximum and minimum stress $R = \frac{\sigma_u}{\sigma_i}$ was either R= 0.1 or R = -1. The stress versus cycles to failure curves measured for composite A are shown in Figure 7. The static strength data show a slightly higher ultimate strength (about 450 MPa) as compared to the tensile tests described earlier in this paper. It is believed that the difference could be caused by the different specimen size (the probed volume was about three times higher in the tensile tests compared to the fatigue tests), statistical uncertainty (only three specimens each were tested) or batch-to-batch variations or a combination thereof. The fact that the specimens used for the cyclic load-unload tests in Figure 2 also fractured at 450 MPa seems to indicate that the specimens for tensile testing were taken from a plate slightly lower infiltration quality.

a)

R=0.1

RT

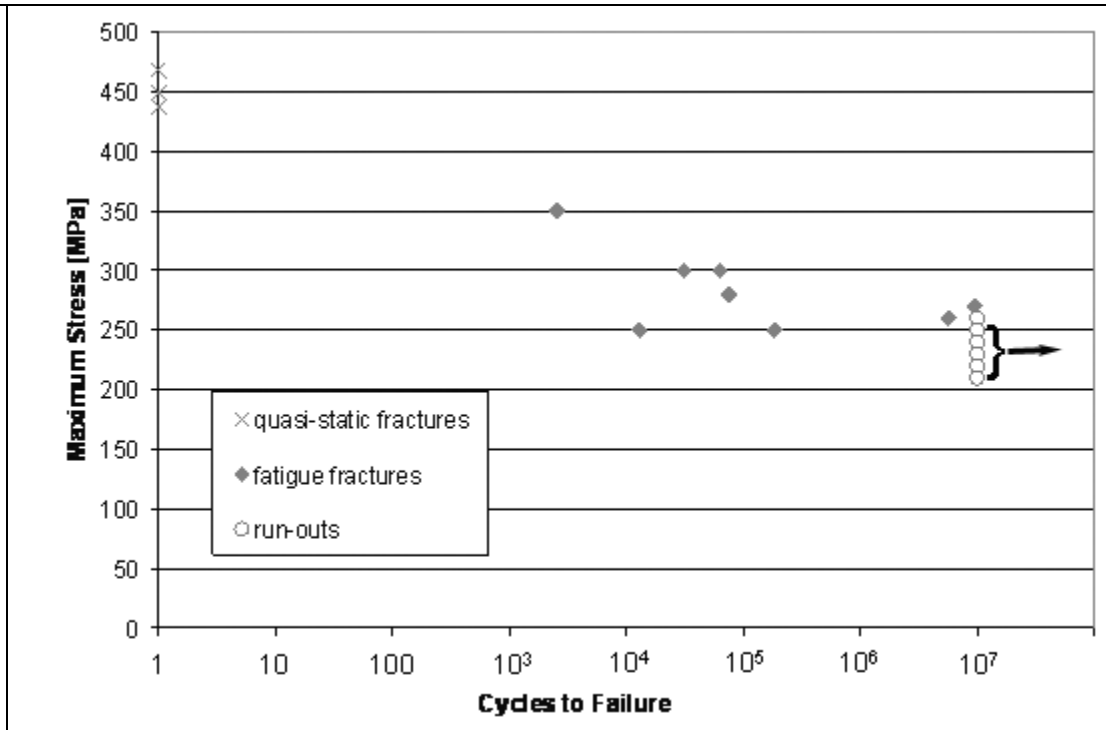

b) R=-1 RT	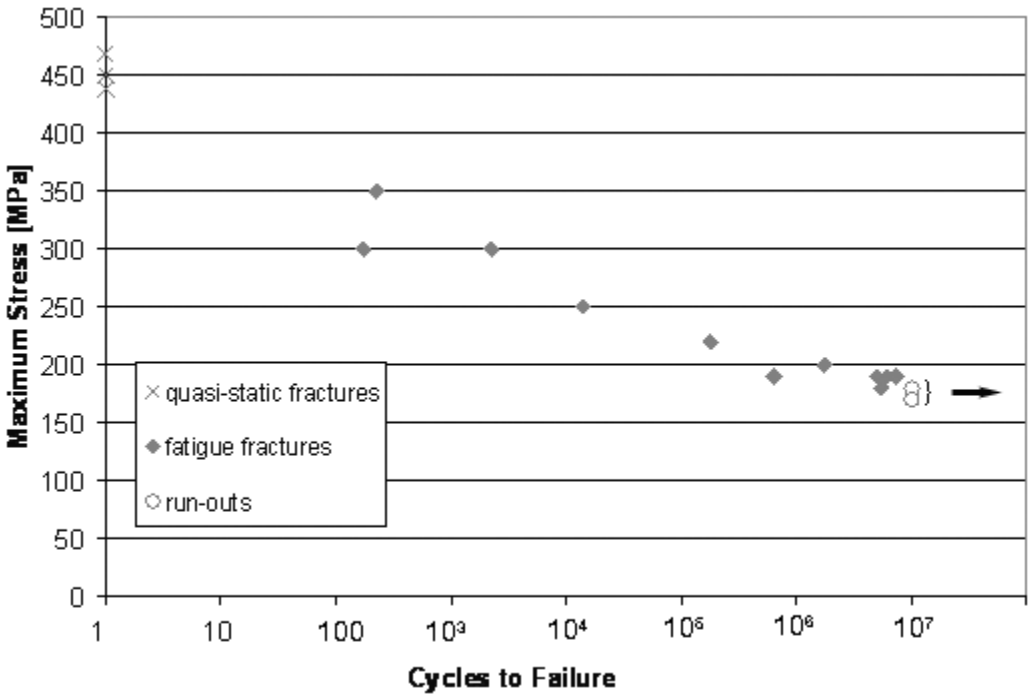
c) R=0.1 150°C	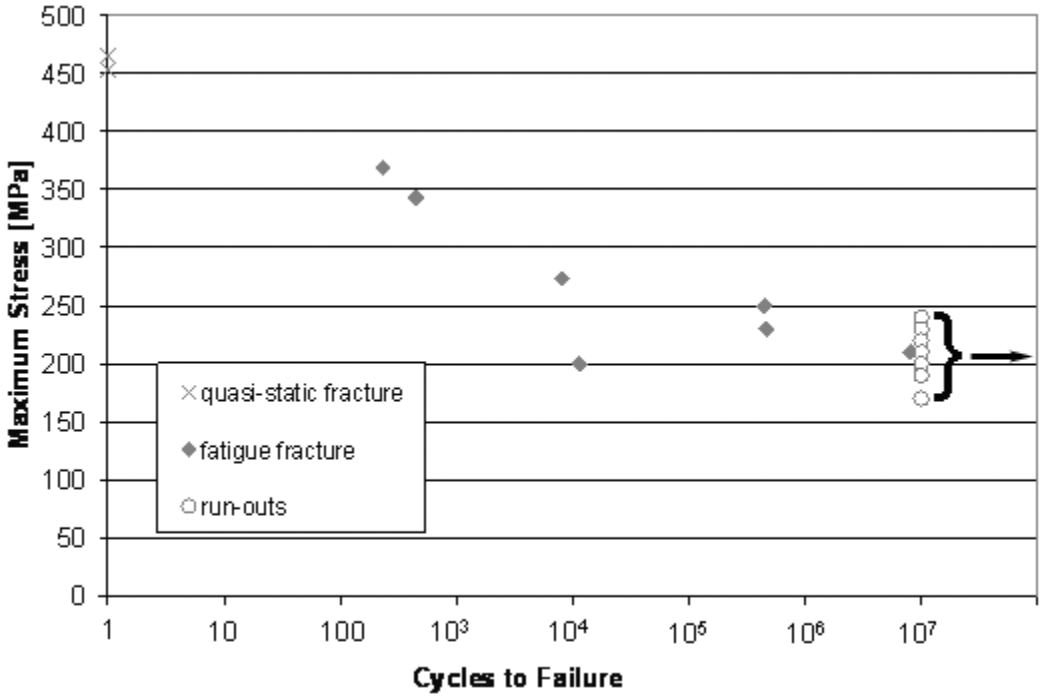

d)

R=-1

150°C

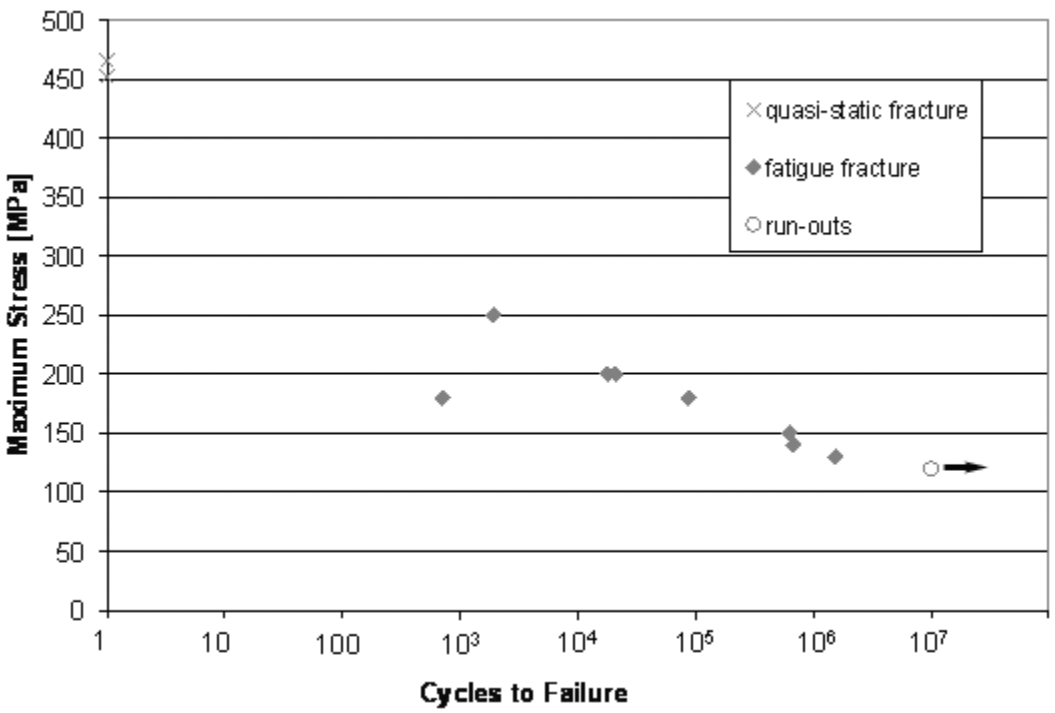

Figure 7: stress versus cycles to failure curves for composite A, a) room temperature, stress-ratio R = 0.1 b) room temperature, stress-ratio R = -1 c) 150°C, stress-ratio R = 0.1 d) 150°C, stress-ratio R = -1

For all stress ratios and temperatures, the strength of composite A decreased significantly with increasing number of load cycles. The dependence of the number of cycles to failure on the applied maximum stress decreased with decreasing applied stress, and a fatigue limit was observed in all cases. This is consistent with observations on AlSi9Cu3 without ceramic reinforcements, where no fatigue fracture was observed below a critical stress intensity factor even for very high cycle numbers up to 10^9 [22]. The fatigue limits of composite A are compared to high-pressure die-cast AlSi9Cu3 and a commercial high-pressure die-cast AlSi9Cu3 alloy reinforced with 20 vol.% SiC particles (Duralcan F3D.20S) in Table 2. The fatigue limits of composite A were 2.3-2.6 times higher (depending on stress ratio) than those of die-cast AlSi9Cu3at room temperature, and about 1.6 times higher than those of die-cast

Duralcan F3D.20S (both at R = 0.1 and R = -1). Similar trends were observed at elevated temperature, but the absolute numbers in Table 2 cannot be directly compared as the testing temperature was 200°C in Ref. 20and 150°C in our experiments.

Table 2: Fatigue limits of composite A compared to high pressure die-cast AlSi9Cu3 and commercial aluminum composite (Duralcan F3D.20S). The fatigue limits for AlSi9Cu3 and F3D.20S are extracted from [20]. Values with asterisks indicate a testing temperature of 200°C

	Fatigue limit (max. stress) for R = 0.1	Fatigue limit (max. stress) for R = 0.1 at 150°C	Fatigue limit (max. stress) for R= -1	Fatigue limit (max. stress) for R = -1 at 150°C
AlSi9Cu3	110 MPa	90 MPa*	69 MPa	52 MPa*
F3D.20S	158 MPa	115 MPa*	117 MPa	55 MPa*
Composite A	248 MPa	210 MPa	182 MPa	110 MPa

Thermophysical Properties

The coefficient of thermal expansion (CTE) of composite A is compared to that of Duralcan F3D.20S in Figure 8. From room temperature up to 250°C, the CTE of composite A is about $15*10^{-6}$ K^{-1} in the temperature range RT to 250°C and thus close to that of many iron alloys which may be useful in cases where the composite has to be joined to such materials. Note that the thermal expansion coefficient is considerably lower than that of Duralcan F3D.20S at any temperature despite of the fact that the alumina reinforcement has a CTE of about $7,1*10^{-6}$ K^{-1} [18], whereas SiC has a CTE of $4.4*10^{-6}$ K^{-1}[19]. The comparatively low CTE of

composite A is partly due to the higher reinforcement content (45 vol% vs 20 vol.% for the Duralcan composite), but also by its interpenetrating microstructure where the ceramic backbone can reduce thermal expansion [20].

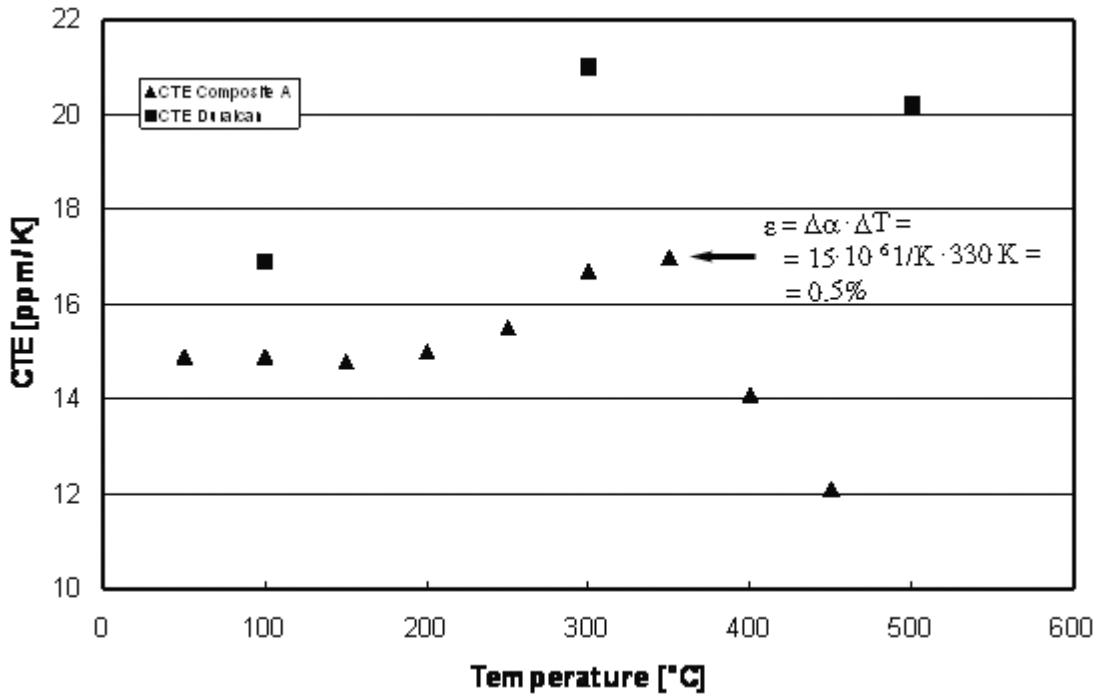

Figure 8: Technical coefficient of thermal expansion of composite A and Duralcan F3D.20S as a function of temperature.

The CTE of composite A decreases rapidly above 350°C. Such a behaviour was also observed in other aluminium-ceramic composites with interpenetrating microstructure and is believed to be related with the formation of micropores in the metal phase due to microstresses during cooling which are closed at high temperatures again [23]. The plastic deformation of the metal induces hysteresis of the thermal macrostrains during a heating/cooling cycle. The drop in CTE in Figure 8 above 350°C is due to the reaching of the yields stress in the matrix. Because of the good bonding between reinforcement and the matrix, the high CTE-mismatch $\Delta\alpha = 15 \cdot 10^{-6}\,K^{-1}$ of AlSi9Cu3 ($22 \cdot 10^{-6}\,K^{-1}$) and alumina ($7 \cdot 10^{-6}\,K^{-1}$) leads to plastic

deformation in the metal matrix at a thermal strain of about 0.5% which corresponds to the UTS of the composite. This observation and explanation is in very good agreement with [24].

The specific heat and the thermal conductivity λ of the composite A is shown in Figure 9. The thermal conductivity was calculated using the thermal diffusivity (determined by laser flash method) a, the specific heat c_p, the density ρ, and the technical CTE α, from room temperature up to 450°C using the relations

$$\lambda(T) = c_p(T) \cdot a(T) \cdot \rho(T) \qquad \text{with} \qquad \rho(T) = \rho(RT) \cdot [1 + \alpha(T) \cdot (T - RT)]^{-3}$$

The results of the measurements are plotted in Figure 9 together with data for Duralcan F3D.20S. The specific heat of composite A and Duralcan F3D.20S is very similar and slightly increases with temperature as expected. The thermal conductivity of composite A is about half the value for the bulk matrix Al alloy found in the literature (between 100 and 120 W/mK [25]). Duralcan F3D.20S also has a higher thermal conductivity than composite A as the SiC reinforcement is a much better heat conductor compared to the alumina reinforcement of composite A. It is interesting to note that the thermal conductivity of composite A is almost independent of temperature (as is the thermal conductivity of the aluminium alloy) whereas the thermal conductivity of alumina decreases from 33 W/mK at room temperature to 11 W/mK at 500°C [18]. It can be concluded that the alumina phase contributes only marginally to the overall conductivity of the composite despite of the interpenetrating network microstructure.

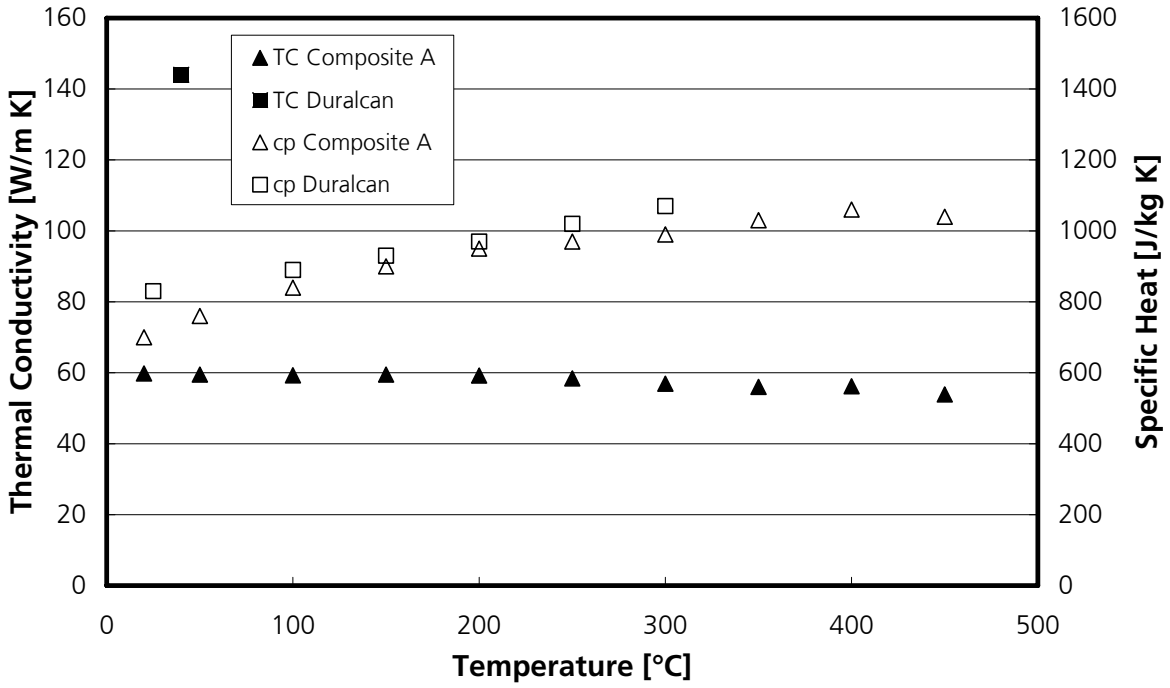

Figure 9: Specific Heat and Thermal conductivity of Composite A and Duralcan F3D.20S as a function of temperature.

Conclusions

Metal ceramic composites produced by infiltration of Al_2O_3 preforms with AlSi9Cu3 show ultimate tensile strengths of up to 450 MPa at a failure strain of up to 0.6% without any heat treatment. The compression strength was up to 850 MPa with 2% strain to failure. The UTS is 2 times higher than for bulk AlSi9Cu3, whereas density is higher by factor of 1.2 only, hence the strength to density ratio for the composites is considerable improved compared to the matrix alloy. The elastic modulus for the Al / Al_2O_3 MMCs determined by a resonance method is 155 GPa, hence again more than 2 times higher than for the bulk AlSi9Cu3. The composites show an excellent resistance to high cycle fatigue with fatigue limits exceeding 200 MPa maximum stress. Fracture surfaces of tensile specimens show cracking of the ceramic reinforcement and a strong interface between ceramic and metal.

Acknowledgement

This work was supported by the Bayerische Forschungsstiftung under the research project "Metallverbunde".

References

[1] K. U. Kainer, in: K.U. Kainer (Ed.), Metal Matrix Composites, Wiley-VCH, Weinheim, 2006, pp. 1-52

[2] H.Y. Wang, Q.C. Jiang, Y.Q. Zhao, Mater Sci Eng A 372 (2004) 109

[3] Z. Trojanova, P. Lukac, W. Riehemann, B.L. Mordike, Mater Sci Eng A 324 (2002) 122

[4] Z.R. Xu, K.K. Chawla, A. Wolfenden, A. Neuman, G.M. Ligget, N. Chawla, Mater Sci Eng A 203 (1995) 75

[5] A. Mattern, B. Huchler, D. Staudenecker, R. Oberacker, A. Nagel, M.J. Hoffmann, J Eur Ceram Soc 24 (2004) 3399

[6] A. M. Samuel, F. H. Samuel, J. Mater. Sci. 29 (1994) 3591-3600

[7] V. Laurent, P. Jarry, G. Regazzoni, D. Apelian, J. Mater. Sci. 27 (1992) 4447

[8] R. Asthana, J. Mater. Sci. 33 (1998) 1679-1698

[9] A. Neubrand, R. Westerheide, B. Thielicke, K.-H. Lang, O. Ulrich, B. Huchler, D. Staudenecker, A. Nagel, Symposium Verbundwerkstoffe und Werkstoffverbunde, in M. Schlimmer (Ed.), Werkstoffinformationsgesellschaft Frankfurt 2005, p. 81-86

[10] S. Wang, H. Geng, Y. Wang, J Mater Sci, 41 (2006) 5751-5757

[11] K. Konopka, A. Olszówka-Myalska, M. Szafran Mater Chem Phys 81 (2003) 239

[12] C. Kammer: Aluminium Taschenbuch, Aluminium Zentrale Düsseldorf, 1998

[13] F. Scherm, R. Völkl, S. van Smaalen, S. Mondal, P. Plamondon, G. L'Espérance F. Bechmann, U. Glatzel, Mater Sci Eng A 518 (2009), 118-123

[14] M. Yamasaki, Y. Kawamura, Scripta Mat 60 (2009) 264

[15] G. S. Daehn, B. Starck, L. Xu, K. F. Elfishawy, J. Ringnalda, H. L. Fraser, Acta mater. 44 (1996) 249-261

[16] J. Lindner, Fatigue Eng Mater, 30 (2007) 759

[17] T.W.Clyne, P.J. Withers, in Chapter 4 of "An Introduction to Metal Matrix Composites", Cambridge University Press 1995

[18] R. G. Munro, J Am Ceram Soc 80 (1997) 1919-1928

[19] R. G. Munro, J Phys Chem Ref Data 26 (1997), 1195-1203

[20] Duralcan Composites for high pressure die castings, Alcan USA, San Diego (1992)

[21] W. Zhou, W. Hu, D. Zhang, Mater Lett, 40 (1999) 156

[22] U. Fuchs, H. Lipowsky, H. Mayer, M. Papakyriacou, A. Stich, S. Tschegg, B. Zettl, Mat.-wiss. u. Werkstofftech., 33 (2002) 117-127

[23] S.Skirl; M Hoffman; K. Bowman; S. Wiederhorn; J. Rödel, Acta Mater. 46, 2493 (1998)

[24] S. Kumar, S. Ingole, H. Dieringa, K.U. Kainer, Compos. Sci. Technol. 63 (2003), 1805-1814

[25] J. M. Holt, Structural Alloys Handbook, CINDAS/Purdue University, West Lafayette 1996